

Measuring Correlations from the Collective Spin Fluctuations of a Large Ensemble of Lattice-Trapped Dipolar Spin-3 Atoms

Youssef Aziz Alaoui^{1,2}, Bihui Zhu,³ Sean Robert Muleady^{4,5}, William Dubosclard,^{1,2} Tommaso Roscilde,⁶
Ana Maria Rey,^{4,5} Bruno Laburthe-Tolra,^{2,1} and Laurent Vernac^{1,2,*}

¹Université Paris 13, Laboratoire de Physique des Lasers, F-93430 Villetaneuse, France

²CNRS, UMR 7538, LPL, F-93430 Villetaneuse, France

³Homer L. Dodge Department of Physics and Astronomy, The University of Oklahoma, Norman, Oklahoma 73019, USA
and Center for Quantum Research and Technology, The University of Oklahoma, Norman, Oklahoma 73019, USA

⁴JILA, NIST and Department of Physics, University of Colorado, Boulder, Colorado 80309, USA

⁵Center for Theory of Quantum Matter, University of Colorado, Boulder, Colorado 80309, USA

⁶Université Lyon, Ens de Lyon, CNRS, Laboratoire de Physique, F-69342 Lyon, France

 (Received 18 January 2022; revised 23 March 2022; accepted 12 May 2022; published 6 July 2022)

We perform collective spin measurements to study the buildup of two-body correlations between $\approx 10^4$ spin $s = 3$ chromium atoms pinned in a 3D optical lattice. The spins interact via long range and anisotropic dipolar interactions. From the fluctuations of total magnetization, measured at the standard quantum limit, we estimate the dynamical growth of the connected pairwise correlations associated with magnetization. The quantum nature of the correlations is assessed by comparisons with analytical short- and long-time expansions and numerical simulations. Our Letter shows that measuring fluctuations of spin populations for $s > 1/2$ spins provides new ways to characterize correlations in quantum many-body systems.

DOI: [10.1103/PhysRevLett.129.023401](https://doi.org/10.1103/PhysRevLett.129.023401)

Introduction.—Experimentally characterizing quantum correlations between different parts of a system is of fundamental importance for the development of quantum technologies. Quantum correlations are not only at the heart of the most peculiar effects predicted by quantum mechanics, such as entanglement, EPR steering [1–3], or Bell nonlocality [4]; they also give advantage for different quantum information or metrological tasks, even for non-entangled states [5–7]. Furthermore, quantum correlations should appear in generic quantum systems [8], and quantum many-body systems are generically intractable by classical computers. Therefore, measurements on well controlled quantum simulators are crucial for improving our understanding of complex quantum systems.

Proving the quantum nature of correlations is an experimental challenge, which requires the measurement of noncommuting operators. As full state tomography scales exponentially with the number of constituents [9] and, thus, becomes impossible in large ensembles, it is of crucial importance to develop new protocols to infer correlations from partial measurements such as bipartite or collective measurements. The latter have been successful in demonstrating entanglement [3], steering [10–12], or nonlocality [13], in experimental platforms dealing with effective two-level systems. Systems made of $s > 1/2$ particles pinned in optical lattices are also particularly interesting for quantum technologies, as their Hilbert space, enlarged with respect to qubit ($s = 1/2$) systems, offers new possibilities for quantum information processing [14]. However, their

entanglement witnesses have a more complicated structure compared to $s = 1/2$ [15–17]. Extensions to $s = 1$ systems in spinor Bose-Einstein condensates have demonstrated number squeezing in pair creation processes via spin-mixing collisions [3,18–21], SU(1,1) interferometry [22], and entangled fragmented phases [23]. Nevertheless, these systems operated in the regime where the single-mode approximation is valid [24], which enormously simplifies the quantum dynamics.

In this Letter, we measure, for the first time, two-body correlations in a macroscopic array of $s = 3$ chromium atoms pinned in a 3D optical lattice and coupled via long-range and anisotropic magnetic dipolar interactions. Previous experiments measuring out-of-equilibrium spin dynamics in these arrays demonstrated beyond mean-field behavior [25,26] and their approach to quantum thermalization [25]. Here, we make use of the large atomic spin to obtain a direct measurement of two-body correlations. Specifically, after triggering out-of-equilibrium spin dynamics, we acquire statistics on the $2s + 1 = 7$ spin populations and quantify the growth of interatomic spin correlations by analyzing the statistical fluctuations of the collective spin component along the external magnetic field, i.e., the magnetization. The quantum nature of the correlations that we measure is validated by agreement with exact short-time expansions, with a high-temperature series expansion applied to the asymptotic quantum thermalized state at long times, and with simulations of the full quantum dynamics via advanced phase-space numerical methods. Thus, our

experimental measurement of a two-body correlator provides a successful test bed for this numerical method in the spirit of quantum simulations.

Proposed correlator.—We consider a system of N spin $s > 1/2$ particles. We define \hat{s}_z^i as the z component of the spin of the i th particle. The correlator C_z that we aim to measure is

$$C_z = \sum_{i \neq j}^N (\langle \hat{s}_z^i \hat{s}_z^j \rangle - \langle \hat{s}_z^i \rangle \langle \hat{s}_z^j \rangle) = \text{Var}(\hat{S}_z) - \Sigma_z, \quad (1)$$

with $\text{Var}(\hat{S}_z) = \langle \hat{S}_z^2 \rangle - \langle \hat{S}_z \rangle^2$ the variance of the collective spin component $\hat{S}_z = \sum_{i=1}^N \hat{s}_z^i$, and Σ_z the sum of individual variances, $\Sigma_z = \sum_{i=1}^N (\langle \hat{s}_z^i \rangle^2 - \langle \hat{s}_z^i \rangle^2)$. Σ_z accounts for intraparticle correlations, which are only nontrivial for $s > 1/2$, as $\langle \hat{s}_z^i \rangle^2 = 1/4$ if $s = 1/2$. The interparticle correlations are accounted for by the two-body correlator C_z . In this Letter, we independently determine $\text{Var}(\hat{S}_z)$ and Σ_z from collective measurements and obtain C_z from Eq. (1). Measurement of $\text{Var}(\hat{S}_z)$ requires the experiment to be repeated many times to acquire adequate statistics (see data analysis below). Measurement of Σ_z is straightforward in the case of a homogeneous system, comprising singly occupied lattice sites (referred to as singlons in the following), as we now explain.

Indeed, for singlons, $\langle \hat{s}_z^i \rangle^2 = \sum_{m_s} p_{m_s}^{(i)} m_s^2$, with $p_{m_s}^{(i)}$ the probability that the site i , uniquely populated by the i th spin, is in the m_s spin state ($-3 \leq m_s \leq 3$, $\sum_{m_s} p_{m_s}^{(i)} = 1$) so that $\sum_i \langle \hat{s}_z^i \rangle^2 = N \sum_{m_s} p_{m_s} m_s^2$ where $p_{m_s} = N^{-1} \sum_i p_{m_s}^{(i)}$. Homogeneity ensures that $p_{m_s}^{(i)} = p_{m_s}$ are independent of site i , so that $\langle \hat{s}_z^i \rangle^2 = (\sum_{m_s} p_{m_s} m_s)^2$; therefore,

$$\frac{\Sigma_z}{N} = \sum_{m_s} p_{m_s} m_s^2 - \left(\sum_{m_s} p_{m_s} m_s \right)^2. \quad (2)$$

In Ref. [27], we show that inhomogeneities lead to negligible deviations from Eq. (2) in our experiment.

Therefore, the measurement of $p_{m_s} = N_{m_s}/N$, with N_{m_s} the total number of atoms in spin state m_s , yields Σ_z , and Eqs. (1), (2) provide a connected two-body correlator by performing measurements in one basis only. Interestingly, in the case of $s > 1/2$, C_z can dynamically evolve in homogeneous systems even when \hat{S}_z commutes with the Hamiltonian.

Experimental setup.—The starting point of our experiments is a spin-polarized ^{52}Cr Bose-Einstein condensate (BEC) produced in a crossed dipole trap, with, typically, 15 000 atoms polarized in the minimal Zeeman energy state $m_s = -3$. We load the ^{52}Cr BEC in a 3D optical lattice deep into the Mott insulator regime. The lattice implemented with five lasers at $\lambda_L = 532$ nm is described in [25]. The total lattice depth is equal to 60 recoil energy at λ_L .

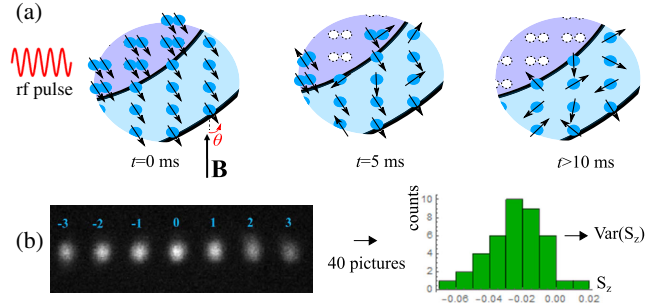


FIG. 1. Principle of the experiment. (a) The cartoons zoom over a small region of the Mott insulating distribution with doubly occupied sites (core) and singly occupied ones (shell). Spin-3 chromium atoms are excited at $t = 0$ by a rf pulse, with five cycles at the Larmor period set by the external magnetic field \mathbf{B} . The spin directions then make an angle θ (set to $\pi/2$ in this Letter) with respect to \mathbf{B} , which triggers spin dynamics. Correlations develop between spins, while doubly occupied sites get empty. (b) Stern-Gerlach separation provides measurement of the fractional spin populations $p_{m_s}(t)$, through fluorescence imaging, at a given time t . Repeating the experiment allows us to compute the variance of the magnetization and, hence, the correlator C_z of Eq. (1).

We estimate the tunneling time to be $\simeq 20$ ms. We obtain a core of doublons comprising $\simeq 50\%$ of the atoms, surrounded by a shell of singlons. Inhomogeneities of the lattice potential are below 2.5% and, therefore, have a negligible effect on spin dynamics in the Mott regime [31].

As shown in Fig. 1(a), we trigger spin dynamics by rotating all spins with the use of a radio frequency (rf) $\pi/2$ pulse. After the pulse, all spins are oriented orthogonal to the external magnetic field, in a coherent spin state. The Larmor frequency $f_L = g_L \mu_B B_0 / \hbar$ (with $g_L \simeq 2$ the Landé factor, μ_B the Bohr magneton, and $B_0 = 0.75$ Gauss the amplitude of the magnetic field) is $f_L \simeq 2.1$ MHz. The rf frequency f_{rf} is set at resonance, and fluctuations of the detuning $(f_L - f_{\text{rf}}) \simeq 1$ kHz are small compared to the rf Rabi frequency f_R , thanks to the use of a 30 Watt rf amplifier. In practice, the rf pulse has a duration of exactly five Larmor periods, with $f_R = (1/5)(f_L/4) = 105$ kHz; the $\bar{\theta} = \pi/2$ pulse is set to have an identical initial phase at each realization. Fluctuations of the rotation angle θ are estimated to have a standard deviation of $\sigma_\theta \simeq 2.5 \times 10^{-3}$ rad (see below). After the initial state preparation with the rf pulse, spins interact via magnetic dipolar interactions in the optical lattice for a duration t . Then, we adiabatically ramp down the optical lattice, and proceed to measurements.

Theoretical models.—Dipolar interactions between singlons during the dark time evolution are described by the effective dipolar Hamiltonian \hat{H}_{dd} , which is a XXZ spin model Hamiltonian

$$\hat{H}_{dd} = \sum_{i>j}^N V_{ij} \left[\hat{s}_z^i \hat{s}_z^j - \frac{1}{2} (\hat{s}_x^i \hat{s}_x^j + \hat{s}_y^i \hat{s}_y^j) \right], \quad (3)$$

with $V_{ij} = V_{dd}(1 - 3\cos^2\theta_{ij}/r_{ij}^3)$, $V_{dd} = (\mu_0(g_L\mu_B)^2/4\pi)$, and μ_0 the magnetic permeability of vacuum. The sum runs over all pairs of particles (i,j) , r_{ij} is their corresponding distance, θ_{ij} the angle between their interatomic axis and the external magnetic field, $\hat{s}_i = \{\hat{s}_x^i, \hat{s}_y^i, \hat{s}_z^i\}$ are $s = 3$ angular momentum operators for atom i . The shortest intersite distance $r_{\min} = 268$ nm in our lattice [25] corresponds to a dipolar coupling $V_{dd}/r_{\min}^3 \simeq h \times 3$ Hz.

Given the strong contact interactions that favor spin alignment [32,33] and the fully polarized initial state, the same Hamiltonian can be used to describe the dynamics of doubly occupied sites (doublons) just by replacing \hat{s}_i by a $s = 6$ angular momentum operator at the corresponding site [31], as the spin of each pair of particles is well-defined. Furthermore, in Ref. [27], we show that Eq. (2) still holds for doubly occupied sites. Nevertheless, as soon as the spin excitation is performed, doublons start to leave the trap due to dipolar relaxation [34], see Fig. 2: for $0 < t < 10$ ms the spin system comprises both singlons and doublons, but only singlons remain for $t > 10$ ms and losses become negligible. This is why we restrict our numerical simulations to the case with singlons only, which allows for quantitative comparison with the experiment except at short times.

As shown in previous work [25], we need to include the one-body term $\hat{H}_Q = B_Q \sum_i^N (\hat{s}_z^i)^2$ accounting for light

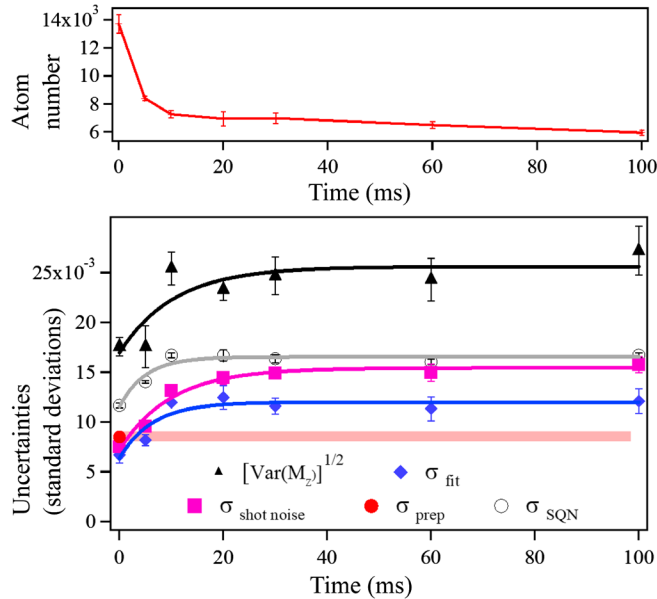


FIG. 2. Evolution of the atom number $N(t)$ (Top), and of the fluctuations measured in the experiment (Bottom): we show the standard deviations of the normalized magnetization M_z and of the technical noises featured in Eq. (4): σ_{prep} (shaded area; preparation of the sample), σ_{fit} (fitting uncertainties), and $\sigma_{\text{shot noise}}$ (fluorescence imaging). The quantum projection noise $\sqrt{(3/2N(t))} = \sigma_{\text{SQN}}$ is shown for comparison. Lines are guides to the eye. Error bars evaluated from statistics correspond to two standard deviations.

shifts created by the lattice lasers. In the Mott regime, tunneling-assisted superexchange processes are happening at longer time scales and remain irrelevant for the current measurements.

During the evolution under $\hat{H}_{dd} + \hat{H}_Q$, $\langle \hat{S}_z \rangle$ and $\text{Var}(\hat{S}_z)$ are constant, as these two operators commute with \hat{S}_z ; on the contrary, interactions between spins lead to evolution of spin populations, hence, of Σ_z and C_z . In our case, as spins are orthogonal to the magnetic field, $\langle \hat{S}_z \rangle = 0$, and Eq. (2) reads $\Sigma_z = N \sum_{m_s} p_{m_s} m_s^2$; moreover, $\text{Var}(\hat{S}_z) = (3/2)N$ as the initial state is a coherent spin state. The short-time evolution is obtained by perturbation theory [25], leading to $C_z \approx -(45N/8)t^2(3V_{\text{eff}}^2 - 4B_Q^2)$, where $V_{\text{eff}}^2 = \sum_{i,j \neq i}^N V_{ij}^2 / (2N)$, $V_{\text{eff}} \simeq h \times 4.3$ Hz. At longer times, we can numerically simulate the dynamics via a semiclassical phase space method known as the generalized discrete truncated Wigner approximation (GDTWA) [35], which was previously shown to capture the spin population dynamics of this system quantitatively [25].

We also provide a theoretical estimate of the expected correlation at long times assuming the eigenstate thermalization hypothesis [9,36]. In this case, due to the build up of quantum correlations, local observables at long times can be described by a thermal density matrix with additional Lagrange multipliers that account for conserved quantities. A high-temperature T series expansion valid for our system [25] leads to $C_z(t \rightarrow \infty) = -(5/2) + 12\beta B_Q N$, with $\beta \equiv (1/k_B T) = (5B_Q + 9\bar{V}/48V_{\text{eff}}^2 + 24B_Q^2)$, and $\bar{V} = (1/N) \sum_{i>j}^N V_{ij} \simeq h \times -0.6$ Hz.

Experimental procedures.—The quantities of interest are the total number of atoms, $N(t)$, and the fractional spin populations $p_{m_s}(t)$. While the fluctuations in $N(t)$ from shot to shot (with a standard deviation of about 10%) yield large extra fluctuations on the measured absolute spin populations $N_{m_s} = N p_{m_s}$, this extra source of noise is canceled when dealing with fractional populations. For measuring the total atom number, we use absorption imaging of the BEC. We checked that the loading in the optical lattice does not lead to losses, and therefore, $N(t=0)$ is equal to the atom number in the BEC. We estimate the accuracy of this measurement to be 10%.

To measure $p_{m_s}(t)$, we spatially separate the seven spin components during a time of flight of 14 ms, using a Stern-Gerlach (SG) technique. We use fluorescence imaging to count atoms, which brings equal efficiency in the detection of all spin components. We also make use of electron multiplying gain, G , which increases the signal-to-noise ratio by effectively eliminating readout noise (see Ref. [27] for details). Atoms are excited by a saturating laser set at 425 nm (with a transition rate $\Gamma = 2\pi \times 5 \times 10^6$ Hz) during typically 500 μs . The magnetic field B_0 is reduced to a small value ($g\mu_B B_0 \ll h\Gamma$) to ensure that the fluorescence rates of the seven spin components are almost equal.

We use a “delta-kick” stage [37] at the very beginning of the time of flight, before SG: it consists of a short 0.5 ms pulse of an intense IR laser along the separation axis of the SG that applies a force on the atoms and helps reduce velocity dispersion. We fine-tune the frequency of the imaging laser and the amplitude of all three components of the magnetic field during the fluorescence stage. The obtained regular shape of clouds [see Fig. 1(b)] favors efficient fitting.

By fitting of the atomic clouds with a Gaussian function, we obtain the values of the number of counts C_{m_s} detected for every spin component m_s which sets the value of $p_{m_s} = C_{m_s} / \sum_{m_s} C_{m_s}$. During the dynamics, $N(t)$ is deduced by multiplying $N(0)$ by the ratio of the total number of counts at t and at $t = 0$.

Data analysis.—As explained above, $\text{Var}(\hat{S}_z)(t)$ is expected to be equal to $(3/2)N(t)$ for a dipolar system without losses, but we do not assume that this equality holds, and we measure $\text{Var}(\hat{S}_z)(t)$ by statistical analysis of the data and thorough investigation of all different sources of parasitic noise. In practice, we measure the variance of the normalized magnetization of the sample, $M_z = \sum_{m_s} p_{m_s} m_s$, $-3 \leq M_z \leq 3$, from three to five sets of 40 pictures. In the absence of noise, $\text{Var}(\hat{S}_z) = N \times \text{Var}(M_z)$, but at $t = 0$, we obtain $N(0) \times \text{Var}(M_z) \simeq 2 \times (3/2)$, which shows that noise processes come into play in our measurement of M_z : a proper determination of $\text{Var}(\hat{S}_z)$ requires an evaluation of their contribution independently.

The noise contributions to M_z originate from fluctuations in the preparation angle θ , in the detection process (due to the Poissonian statistics of light) and in the evaluation of counts on the camera (related to error in the fitting procedure). We denote their respective contribution to the standard deviation on M_z as σ_{prep} , $\sigma_{\text{shot noise}}$, and σ_{fit} . These different noise sources are statistically independent, so that

$$\text{Var}[M_z(t)] = \frac{\text{Var}[\hat{S}_z(t)]}{N^2(t)} + \sigma_{\text{shot noise}}^2(t) + \sigma_{\text{fit}}^2(t) + \sigma_{\text{prep}}^2, \quad (4)$$

from which we derive $\text{Var}(\hat{S}_z)(t)$ at any time t .

We determine $\sigma_{\text{shot noise}}$ from the fundamental fluctuations of the fluorescence signal of each spin components (with a corresponding standard deviation $\sqrt{2GC_{m_s}}$, see Ref. [27]). Similarly, σ_{fit} is well evaluated from data analysis. We use measurements at $t = 0$ to evaluate the last contribution, σ_{prep} . Indeed, the initial sample corresponds to an uncorrelated spin coherent state, for which $\text{Var}(\hat{S}_z) = (3/2)N(0)$ is guaranteed. The conservation of magnetization during the whole spin dynamics ensures that σ_{prep} is constant, as discussed in [27]; we stress that the

contribution of the preparation noise becomes negligible at long times, see Fig. 2.

The noise contributions as dynamics proceeds are shown in Fig. 2, and compared to the one of atomic projection noise, $\sigma_{\text{SQN}} = \sqrt{(3/2)N(t)}$. We obtain $\sigma_{\text{prep}} = 0.008 \simeq 0.7\sigma_{\text{SQN}}$. As σ_{prep} scales like $s \times g_L$ and is independent of N_0 , while σ_{SQN} scales like $\sqrt{(s/N(0))}$, we stress the difficulty to get such a low value for a large $N(0)$, a large spin $s = 3$ and a large Landé factor $g_L = 2$. The increase of $\sigma_{\text{shot noise}}$ as a function of time (see Fig. 2) surpasses the $1/\sqrt{N(t)}$ scaling due to the increasing contribution of the highest $|m_s|$ states; the increase of σ_{fit} stems from atom losses.

Results.—We show our measurements of $\text{Var}(\hat{S}_z)(t)/N(t)$ in Fig. 3(a). The scatter of the data points around $(3/2)$ is

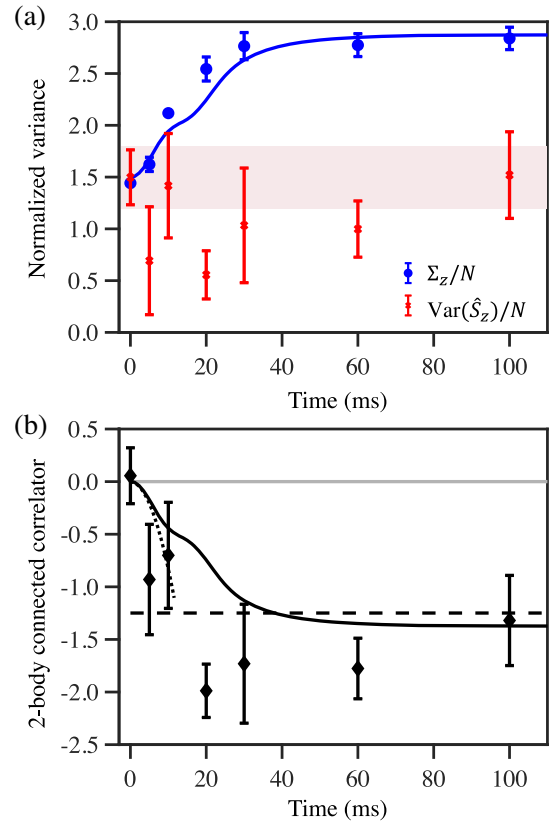


FIG. 3. (a) Symbols are experimental values for the two contributions to the correlator C_z [see Eq. (1)] normalized to atom number. Full line is results of simulations for Σ_z , while the shaded area shows the expected values for $\text{Var}(\hat{S}_z)$ in a pure dipolar spin system within 2 standard deviations, as a result of our finite data sampling. (b) Experimental values of the correlator C_z normalized to the atom number (symbols), with comparison to simulations (full line), and short-time expansion (dotted line). The dashed line corresponds to the calculated value in the quantum thermalized state, while the light grey line shows the zero value. Error bars evaluated from statistics correspond to two standard deviations.

comparable to the average error bars for the different points. Therefore, our measurements are statistically compatible with $(3/2)$ throughout the curve. We point out that the experimental error bars are similar to the expected fluctuations on the measurement associated with finite data sampling, which we have estimated at $t = 0$ with random choice numerical simulations for 200 shots, see Fig. 3(a).

As we measure a substantial growth for $\Sigma_z(t)/N(t)$, we can assert that the correlator $C_z(t)$ significantly differs from zero for $t > 20$ ms, as directly shown in Fig. 3(b). At the asymptotic time $t = 100$ ms, our measurement shows incompatibility of C_z with zero with a confidence interval larger than 99%. Figure 3(a) shows a good quantitative agreement between the measured $\Sigma_z(t)/N(t)$ and predictions from our GDTWA simulations assuming only singlons, while Fig. 3(b) shows qualitative agreement for the measured $C_z(t)$ with our short-time expansion. The value of the quadratic term B_Q in simulations, $B_Q = \hbar \times -5.1$ Hz, is inferred from population analysis during the whole dynamics [27]; it leads to $(C_z/N)(t \rightarrow \infty) \simeq -1.3$, in good agreement with the data. Thus, our measurement results confirm the ability of GDTWA to estimate the growth of correlations for large ensembles of large spins atoms.

Discussion and conclusions.—Thus, our measurements quantify the amount of two-body correlations in the expected highly correlated state reached at long time. Assuming translational invariance and isotropic correlations decaying exponentially with a correlation length ξ , the measured C_z and Σ_z at long time can be related to the onset of correlations with $\xi \approx 0.3$ (in units of the lattice spacing) [27]. This estimate represents a lower bound to the actual correlation length (assuming concentration of correlations at short distance); its rather small value is, nonetheless, compatible with the scenario of thermalization at high temperature.

Now, we discuss the influence of losses. As dipolar spin exchange dynamics proceeds, doublons can become correlated with surrounding singlons, resulting in a modification of singlon fluctuations. Therefore, quantum fluctuations of the sample, and consequently its quantum correlations, may differ from the singlon-only case. Rigorously taking losses into account is difficult and would require new theoretical models to be developed, which is beyond the scope of this Letter. We discuss simple arguments in [27] to estimate the contribution of losses on $\text{Var}(\hat{S}_z)(t)$ and predict small corrections at the 10 percent level. An improved experimental resolution would be necessary to show deviation from a fully unitary system. However, our experimental results show that the growth of correlations is not significantly hampered by dipolar losses—an example of the strength of the quantum simulation approach when theoretical models are not yet available.

In conclusion, we have measured the growth of correlations in a large ensemble of interacting spins by analyzing the fluctuations of the collective magnetization. This

achievement illustrates the new possibilities offered by $s > 1/2$ species, for which relevant information can be accessed by measuring population fluctuations in one basis. This paves the way for a better understanding of the dynamics of quantum correlations in nonequilibrium spin systems.

We acknowledge careful review of this manuscript and useful comments from Thomas Bilitewski and Lindsay Sonderhouse. The Villetaneuse group and Lyon group acknowledge financial support from CNRS, Conseil Régional d’Ile-de-France under Sirteq Agency, Agence Nationale de la Recherche (Projects No. EELS—ANR-18-CE47-0004), and No. QuantERA ERA-NET (MAQS Project). A. M. R. is supported by the AFOSR Grant No. FA9550-18-1-0319, AFOSR MURI, by the DARPA DRINQs Grant, the ARO single investigator Grant No. W911NF-19-1-0210, the NSF Grants No. PHY1820885 and No. NSF JILA-PFC PHY-1734006, and by NIST.

*Corresponding author.

laurent.vernac@univ-paris13.fr

- [1] R. Horodecki, P. Horodecki, M. Horodecki, and K. Horodecki, Quantum entanglement, *Rev. Mod. Phys.* **81**, 865 (2009).
- [2] D. Cavalcanti and P. Skrzypczyk, Quantum steering: A review with focus on semidefinite programming, *Rep. Prog. Phys.* **80**, 024001 (2017).
- [3] L. Pezzè, A. Smerzi, M. K. Oberthaler, R. Schmied, and P. Treutlein, Quantum metrology with nonclassical states of atomic ensembles, *Rev. Mod. Phys.* **90**, 035005 (2018).
- [4] N. Brunner, D. Cavalcanti, S. Pironio, V. Scarani, and S. Wehner, Bell nonlocality, *Rev. Mod. Phys.* **86**, 419 (2014).
- [5] H. Ollivier and W. H. Zurek, Quantum Discord: A Measure of the Quantumness of Correlations, *Phys. Rev. Lett.* **88**, 017901 (2001).
- [6] S. Luo, Quantum discord for two-qubit systems, *Phys. Rev. A* **77**, 042303 (2008).
- [7] A. Bera, T. Das, D. Sadhukhan, S. S. Roy, A. Sen(De), and U. Sen, Quantum discord and its allies: A review of recent progress, *Rep. Prog. Phys.* **81**, 024001 (2018).
- [8] A. Ferraro, L. Aolita, D. Cavalcanti, F. M. Cucchietti, and A. Acín, Almost all quantum states have nonclassical correlations, *Phys. Rev. A* **81**, 052318 (2010).
- [9] A. M. Kaufman, M. E. Tai, A. Lukin, M. Rispoli, R. Schittko, P. M. Preiss, and M. Greiner, Quantum thermalization through entanglement in an isolated many-body system, *Science* **353**, 794 (2016).
- [10] M. Fadel, T. Zibold, B. Décamps, and P. Treutlein, Spatial entanglement patterns and Einstein-Podolsky-Rosen steering in Bose-Einstein condensates, *Science* **360**, 409 (2018).
- [11] P. Kunkel, M. Prüfer, H. Strobel, D. Linnemann, A. Frölian, T. Gasenzer, M. Gärtner, and M. K. Oberthaler, Spatially distributed multipartite entanglement enables EPR steering of atomic clouds, *Science* **360**, 413 (2018).
- [12] K. Lange, J. Peise, B. Lücke, I. Kruse, G. Vitagliano, I. Apellaniz, M. Kleinmann, G. Tóth, and C. Klempt, En-

- tanglement between two spatially separated atomic modes, *Science* **360**, 416 (2018).
- [13] R. Schmied, J.-D. Bancal, B. Allard, M. Fadel, V. Scarani, P. Treutlein, and N. Sangouard, Bell correlations in a Bose-Einstein condensate, *Science* **352**, 441 (2016).
- [14] Y. Wang, Z. Hu, B. C. Sanders, and S. Kais, Qudits and high-dimensional quantum computing, *Front. Phys.* **8**, 479 (2020).
- [15] A. S. Sørensen and K. Mølmer, Entanglement and Extreme Spin Squeezing, *Phys. Rev. Lett.* **86**, 4431 (2001).
- [16] G. Vitagliano, P. Hyllus, I. L. Egusquiza, and G. Tóth, Spin Squeezing Inequalities for Arbitrary Spin, *Phys. Rev. Lett.* **107**, 240502 (2011).
- [17] G. Vitagliano, I. Apellaniz, I. L. Egusquiza, and G. Tóth, Spin squeezing and entanglement for an arbitrary spin, *Phys. Rev. A* **89**, 032307 (2014).
- [18] E. M. Bookjans, C. D. Hamley, and M. S. Chapman, Strong Quantum Spin Correlations Observed in Atomic Spin Mixing, *Phys. Rev. Lett.* **107**, 210406 (2011).
- [19] C. Gross, H. Strobel, E. Nicklas, T. Zibold, N. Bar-Gill, G. Kurizki, and M. K. Oberthaler, Atomic homodyne detection of continuous-variable entangled twin-atom states, *Nature (London)* **480**, 219 (2011).
- [20] B. Lücke, M. Scherer, J. Kruse, L. Pezzé, F. Deuretzbacher, P. Hyllus, O. Topic, J. Peise, W. Ertmer, J. Arlt, L. Santos, A. Smerzi, and C. Klempt, Twin matter waves for interferometry beyond the classical limit, *Science* **334**, 773 (2011).
- [21] A. Qu, B. Evrard, J. Dalibard, and F. Gerbier, Probing Spin Correlations in a Bose-Einstein Condensate Near the Single-Atom Level, *Phys. Rev. Lett.* **125**, 033401 (2020).
- [22] D. Linnemann, H. Strobel, W. Muessel, J. Schulz, R. J. Lewis-Swan, K. V. Kheruntsyan, and M. K. Oberthaler, Quantum-Enhanced Sensing Based on Time Reversal of Nonlinear Dynamics, *Phys. Rev. Lett.* **117**, 013001 (2016).
- [23] B. Evrard, A. Qu, J. Dalibard, and F. Gerbier, Observation of fragmentation of a spinor Bose-Einstein condensate, *Science* **373**, 1340 (2021).
- [24] C. K. Law, H. Pu, and N. P. Bigelow, Quantum Spins Mixing in Spinor Bose-Einstein Condensates, *Phys. Rev. Lett.* **81**, 5257 (1998).
- [25] S. Lepoutre, J. Schachenmayer, L. Gabardos, B. H. Zhu, B. Naylor, E. Maréchal, O. Gorceix, A. M. Rey, L. Vernac, and B. Laburthe-Tolra, Exploring out-of-equilibrium quantum magnetism and thermalization in a spin-3 many-body dipolar lattice system, *Nat. Commun.* **10**, 1714 (2019).
- [26] A. Patscheider, B. Zhu, L. Chomaz, D. Petter, S. Baier, A.-M. Rey, F. Ferlaino, and M. J. Mark, Controlling dipolar exchange interactions in a dense three-dimensional array of large-spin fermions, *Phys. Rev. Research* **2**, 023050 (2020).
- [27] See Supplemental Material <http://link.aps.org/supplemental/10.1103/PhysRevLett.129.023401> for details on experimental procedure and simulations, which includes Refs. [28–30].
- [28] K. Kechadi, Analyse theorique des excitations et des instabilites des condensats de bose-einstein spinoriels dipolaires, Ph.D. thesis, Université Paris 13, 2019, https://tel.archives-ouvertes.fr/tel-02386895v2/file/these_kechadi_kaci.pdf.
- [29] B. Pasquiou, G. Bismut, Q. Beauvils, A. Crubellier, E. Maréchal, P. Pedri, L. Vernac, O. Gorceix, and B. Laburthe-Tolra, Control of dipolar relaxation in external fields, *Phys. Rev. A* **81**, 042716 (2010).
- [30] M. Robbins and B. Hadwen, The noise performance of electron multiplying charge-coupled devices, *IEEE Trans. Electron Devices* **50**, 1227 (2003).
- [31] P. Fersterer, A. Safavi-Naini, B. Zhu, L. Gabardos, S. Lepoutre, L. Vernac, B. Laburthe-Tolra, P. B. Blakie, and A. M. Rey, Dynamics of an itinerant spin-3 atomic dipolar gas in an optical lattice, *Phys. Rev. A* **100**, 033609 (2019).
- [32] S. Lepoutre, K. Kechadi, B. Naylor, B. Zhu, L. Gabardos, L. Isaev, P. Pedri, A. M. Rey, L. Vernac, and B. Laburthe-Tolra, Spin mixing and protection of ferromagnetism in a spinor dipolar condensate, *Phys. Rev. A* **97**, 023610 (2018).
- [33] S. Lepoutre, L. Gabardos, K. Kechadi, P. Pedri, O. Gorceix, E. Maréchal, L. Vernac, and B. Laburthe-Tolra, Collective Spin Modes of a Trapped Quantum Ferrofluid, *Phys. Rev. Lett.* **121**, 013201 (2018).
- [34] A. de Paz, A. Chotia, E. Maréchal, P. Pedri, L. Vernac, O. Gorceix, and B. Laburthe-Tolra, Resonant demagnetization of a dipolar Bose-Einstein condensate in a three-dimensional optical lattice, *Phys. Rev. A* **87**, 051609(R) (2013).
- [35] B. Zhu, A. M. Rey, and J. Schachenmayer, A generalized phase space approach for solving quantum spin dynamics, *New J. Phys.* **21**, 082001 (2019).
- [36] L. D'Alessio, Y. Kafri, A. Polkovnikov, and M. Rigol, From quantum chaos and eigenstate thermalization to statistical mechanics and thermodynamics, *Adv. Phys.* **65**, 239 (2016).
- [37] H. Ammann and N. Christensen, Delta Kick Cooling: A New Method for Cooling Atoms, *Phys. Rev. Lett.* **78**, 2088 (1997).